

Silica Cross-Linked Micellar Core–Shell Nanoparticles Encapsulating IR-780 with Strong Bright and Good Biocompatibility for Optical Imaging *In Vivo*

Yonghua Zhan^{1,†}, Xu Cao^{1,†}, Xin Cao¹, Yingchao Li¹, Jie Tian², Jimin Liang^{1,*}, and Xueli Chen^{1,*}

¹*Engineering Research Center of Molecular and Neuro Imaging of the Ministry of Education,
 School of Life Science and Technology, Xidian University, Xi'an, Shaanxi 710071, China*

²*Institute of Automation, Chinese Academy of Sciences, Beijing 100190, China*

IR-780 iodide, a near-infrared (NIR) fluorescent heptamethine dye, has attracted wide attention in the biomedical community. However, hydrophobicity and toxicity severely limit its further biomedical application. Although many successful efforts have been made to increase its solubility and biocompatibility, a strong fluorescent signal and longer retention time are in high demand in biomedical application *in vivo* as well as basic science research. In this work, we report the development of novel silica cross-linked micellar core–shell nanoparticles encapsulating IR-780 (NIR-Silica NPs) and their utility for biomedical imaging *in vivo*. Compared to free IR-780, the solubility of NIR-Silica NPs was not only greatly increased, but there was also a dramatic 5–7-fold enhancement of fluorescence intensity. More importantly, the exceptionally small size (25 nm) and colloidal stability of the NPs are also sufficient to realize the enhanced permeability and retention effect. *In vitro* cell viability assays further indicated that the NIR-Silica NPs are safer even at the highest concentration tested of 1.0 mg/mL. Finally, sentinel lymph node mapping and long-term tumor imaging *in vivo* demonstrated that the NIR-Silica NPs have a long circulation time and higher signal-to-noise ratio at a very low dye concentration and short exposure time (0.2 s). Therefore, the NIR-Silica NPs may be a promising fluorescence imaging agent for clinical application.

KEYWORDS: *Near-Infrared, Heptamethine Dye, Cross-Linked, Silica, Fluorescence, Optical Imaging.*

INTRODUCTION

Optical imaging is a promising noninvasive, real-time and high-resolution molecular imaging approach widely used in brain functional imaging,¹ drug delivery,^{2,3} tumor targeting,^{4,5} photothermal therapy (PTT), photodynamic therapy (PDT),⁶ imaging-guided surgery⁷ and sentinel lymph node (SLN) mapping fields.^{8,9} NIR fluorescence is an optical imaging technology which has received immense attention because of its low absorption and autofluorescence from tissues and organisms within the NIR spectral range of 700–1000 nm, which can improve tissue depth penetration and image sensitivity.¹⁰ Quantum dots (QDs), up-conversion particles (UCNP) and organic NIR fluorescence dyes are current NIR probes

which have rapidly emerged as fluorescence probes for imaging of biological samples *in vitro* and *in vivo*.¹¹ However, QDs and UCNPs have toxic heavy metal elements in their cores, which make the safety of these nanoparticles (NPs) a serious concern in biological applications, and thus have prevented their further application in clinical imaging. IR-780 iodide, as an organic NIR fluorescent agent, is a lipophilic cationheptamethine dye with high fluorescence intensity due to the rigid cyclohexenyl ring in the heptamethine chain.¹² To date, IR-780 has been widely used for PDT and PTT, in which the dye is employed as a clinical therapeutic agent due to its ability to generate singlet oxygen and produce heat after laser irradiation.¹³ In addition, IR-780 also showed preferential accumulation in multiple tumor cells due to its affinity for organic anion transporter peptides (OATP).¹⁴ However, IR-780 is extremely difficult to dissolve in a pharmaceutically acceptable solvent, which severely limits its further biological and clinical application.

*Authors to whom correspondence should be addressed.

Emails: jimleung@mail.xidian.edu.cn, xlchen@xidian.edu.cn

†These two authors contributed equally to this work.

Received: 18 December 2015

Revised/Accepted: 18 August 2016

To improve the utility of IR-780 for optical imaging and therapeutic application, much recent research has been dedicated to overcome these disadvantages by encapsulating IR-780 into various nanocarriers. For example, polymeric micelles labeled with the radionuclide rhenium-188,¹⁵ heparin-folic acid NPs¹⁶ and PEG-IR-780-C13 micelles¹⁷ were all self-assembled to improve the water solubility of IR-780. Although the solubility of IR-780 has been dramatically improved, the photo-physical stability and fluorescence intensity of the dye decreased due to either complicated synthesis or repeated laser irradiation. In another approach, human serum albumin NPs were developed to increase the water solubility of IR-780.¹⁸ However, the large size of these NPs may lead to clearance by the reticuloendothelial system (RES) and their relatively weak fluorescence intensity is not sufficient for PTT and PDT. Engineering mesoporous silica NPs was carried out to integrate IR-780 into a silica matrix to improve solubility.¹⁹ However, this led to a low fluorescence intensity of IR-780. Of course, to some extent, NIR dyes with a good fluorescence quantum yield in non-polar media including IR-780 generally demonstrate lower fluorescence efficiency in aqueous environments. However, the fluorescence intensity of NIR dyes in an aqueous solution can also be enhanced. Therefore, the development of a simple and robust method for delivering IR-780 as an ideal NIR imaging probe for clinical application is urgent. This not only should increase water solubility but also meet at least the following general criteria:

- (a) smaller size and longer retention time;
- (b) safe and non-toxic to hosts; and
- (c) sufficient photo-physical stability and a strong fluorescent signal.

Polymeric micelles as drug agent or dye carriers are inexpensive to synthesis and are available in large quantities for biomedical applications.²⁰ However, the physical stability of the polymeric micelles is a critical problem. A recent study has shown that the *in vivo* biological effect of drugs or dyes incorporated into polymeric micelles is positively correlated with micelle stability.²¹ While polymeric micelles may be unstable *in vivo* environments, we must emphasize that polymeric micelles are still versatile and may be a cost-effective approach for delivering IR-780.²² In order to make full use of polymeric micelles as an IR-780 carrier, the most widely used method to solve this problem is to introduce cross-linking functional groups with the core or shell of polymeric micelles through the synthesis process. However, this method requires multiple synthetic steps, which limits its application to some extent.²³ On the other hand, silica cross-linking (SSCL) polymeric micelles have become popular in recent years. Silica has been extensively employed due to its rich surface chemistry as well as being non-toxic and biocompatible, as proven by the U.S. Food and Drug Administration.²⁴ Additionally, silica cross-linking could provide further advantages, such as mild and simple synthesis, maintenance of stability against dilution and temperature fluctuations, tunable size and improvement in the photo-stability of fluorescent agent by reducing their contact with the outside environment.^{25–28} These benefits inspired us to further explore strategies that could increase IR-780 water solubility and photo-physical stability.

In this study, we developed a novel and robust method to develop a new family of biocompatible silica cross-linked micellar encapsulating IR-780 nanoparticles (NIR-Silica NPs), which were synthesized by modifying a bio-inspired

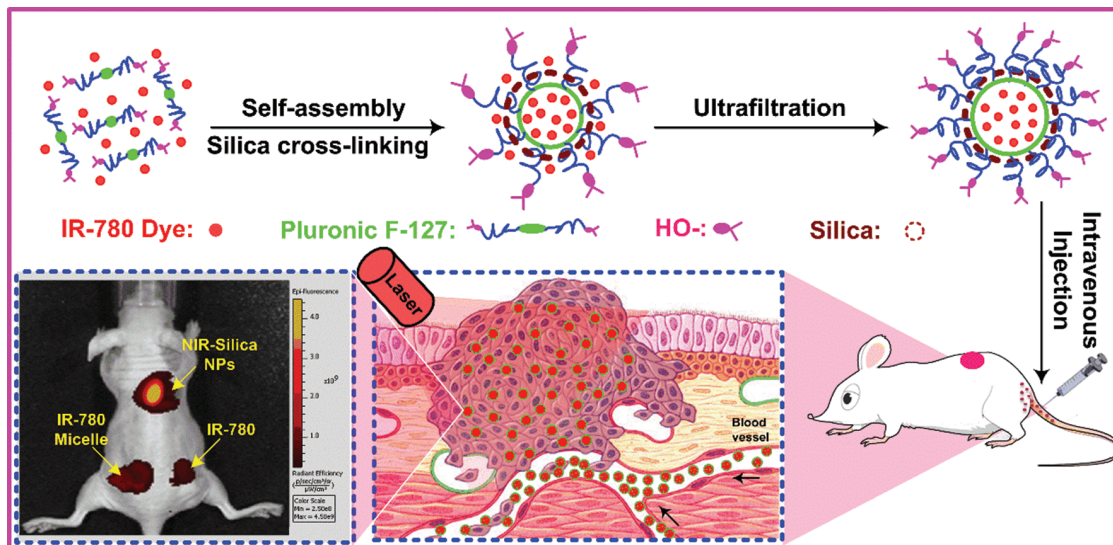


Figure 1. Schematic of NIR-Silica NPs formation and tumor imaging by NIR-Silica NPs. IR-780 was self-assembled by using pluronic F-127. The pluronic F-127 micelle was then cross-linked with silica physically between the core and the shell of the F-127 polymeric micelles simultaneously. The silica and pluronic F-127 provide a better capability and higher stability than free IR-780. NIR-Silica NPs show a strong and bright signal for optical imaging *in vivo* with short exposure times at low dye concentrations.

silification method (Fig. 1). The process was simple and robust enough to simultaneously encapsulate IR-780 into the core of the pluronic F-127 polymeric micelles and form a thin silica layer between the core and the shell of the polymeric micelles. Properties such as ultraviolet (UV) absorption spectra, fluorescence emission spectra, morphology, stability and size distribution were investigated. The enhancement of fluorescent intensity and tissue penetration of NIR-Silica NPs were studied *in vitro* and *in vivo*. In addition, their cytotoxicity was also investigated using HEK293 and A431 cell lines, through MTT assays. Finally, a series of experiments including SLN mapping and long-term tumor imaging were performed to evaluate the circulation time and signal-to-noise ratio *in vivo*.

MATERIALS AND METHODS

Materials

Pluronic F-127 ($\text{PEO}_{100}-\text{PPO}_{65}-\text{PEO}_{100}$, average MW ~ 12600) was obtained from BASF Corp. (Mount Olive, NJ). Tetraethylorthosilicate (TEOS, 99.99%), diethoxydimethylsilane (DEDMS, 97%) and IR-780 iodide were purchased from Sigma-Aldrich Corp. (St. Louis, MO). Hydrochloric acid (37%), dichloromethane and chloroform were purchased from Tianjin Chemical Ltd. (Tianjin, China). Thiazolylblue tetrazolium bromide (MTT) was purchased from Invitrogen (Carlsbad, CA). Cell culture medium (RPMI 1640, complete DMEM high glucose), trypsin (for cell culture use, 0.25% w/v), and fetal bovine serum (FBS) were purchased from Thermo Fisher Scientific Co., Ltd. (Shanghai, China). The tumor cell lines A431 and HEK293 were provided by the School of Life Science and Technology, Xi'an Jiaotong University. All reagents and solvents were used as received without further purification.

Preparation of NIR-Silica NPs

The synthesis steps for NIR core–shell silica-pluronic NPs are shown in Figure 1. In a typical preparation, 120 mg pluronic F-127 and 0.5 mg IR-780 iodide were carefully co-solubilized with 2 mL dichloromethane in a 20 mL glass scintillation vial. The solvent was evaporated to form the homogeneous solution by means of gentle nitrogen flow under a vacuum at room temperature. The solid residue was then solubilized by magnetic stirring with 1560 μL of 0.85 M HCl. The undissolved materials were discarded after centrifugation and the IR-780 micelle solution was formed; then, the solution was transferred into a new 20 mL glass scintillation vial. TEOS (180 μL , 0.81 mmol) was then added to the resulting aqueous solution followed by DEDMS (15 μL , 0.09 mmol) after 120 min. The mixture was continuously stirred for 20 h at 25 °C before dialysis. The dialysis purification was carried out using a precise amount of NPs solution (15 mL) which was finally diluted with water to a total volume of 30 mL. The concentration of the dye within NPs

was determined using a UV-NIR spectrometer (DU730, Beckman, USA).

Characterization of NIR-Silica NPs

The size distribution of the NIR-Silica NPs was measured by dynamic light scattering using a Malvern instruments Nano-ZS90 machine (Malvern, UK). The concentration of the NIR-Silica NPs was 0.5% in water, and the temperature was controlled at 25 °C. For each sample, the size distribution measurement was performed for fifteen cycles per run. To further examine the morphology of NPs, a JEOL 2010F transmission electron microscope (TEM) (Tokyo, Japan) was used. The NPs solution (1 mg/mL) was poured onto a 400 mesh carbon coated copper grid and dried at room temperature. Then, the sample was observed by the TEM instrument at 100 kV. To determine the dye content of the NIR-Silica NPs, the absorption spectra of NIR-Silica NPs, IR-780 micelle and freely dissolved IR-780 dye were obtained using a UV-NIR spectrometer. The above NIR-Silica NPs and IR-780 micelle solution (50 μL) was added to 950 μL of dimethylsulfoxide (DMSO) as the experimental sample respectively. The DMSO solution with the same concentration of IR-780 was used as a control. A solution of 50 μL of deionized water plus 950 μL of DMSO was used as a blank. The equivalent IR-780 concentration of the NIR-Silica NPs and IR-780 micelle solution was determined by comparing the absorbance of the NIR-Silica NPs in DMSO at 792 nm to a standard absorption curve of free IR-780 dye in the same solution. All measurements were performed in triplicate. Fourier Transform Infrared Spectroscopy (FTIR) was recorded using a Thermo Scientific TIR instrument (Nicolet 8700) using KBr pellet techniques. TGA curves were recorded using a TA instrument (TGA-2900 model) under N_2 . The encapsulation efficiency (EE) and Dye loading (DL) of the IR-780 dye in NIR-Silica NPs were calculated using the following formulas:

$$\text{Encapsulation efficiency}_{\text{dye}} (\%) = \frac{C_{\text{dye remain}}}{C_{\text{dye input}}} \times 100\% \quad (1)$$

$$\text{Dye loading}_{\text{dye}} (\%) = \frac{C_{\text{dye remain}}}{C_{\text{NIR-Silica NPs input}}} \times 100\% \quad (2)$$

In Vitro Release Profiles and Stability of NIR-Silica NPs

The IR-780-release profile of NIR-Silica NPs was measured using a dialysis membrane (MWCO ~ 3500) stirred at 30 rpm and 37 °C for 72 h in a release buffer containing 0.2% Tween-80 and 0.5% BSA in a PBS solution (pH 7.4). The amounts of free IR-780 dye in the sample solutions were determined using a UV spectrophotometer after dialysis was completed. The same amounts of free IR-780 and IR-780 micelle samples obtained under the same conditions were used as controls. The stability of NIR-Silica NPs and their size distribution were measured

regularly using restored samples in PBS and 10% FBS at different times and temperatures after 2 weeks. All of the data above are presented as means \pm SD ($n = 3$).

Cytotoxicity of NIR-Silica NPs *In Vitro*

The cytotoxicity of NIR-Silica NPs was assessed with a methyl tetrazolium (MTT) viability assay using A431 cells and HEK 293 cells. The cells were seeded in 96-well plates at 20,000 cells per well in a 200 μ L culture medium. The cells were maintained in DMEM containing 10% fetal bovine serum, supplemented with 100 U mL⁻¹ penicillin and 100 U mL⁻¹ streptomycin, and incubated at 37 °C in a humidified cell culture incubator (MCO-20AIC, Sanyo, Japan) with 5% CO₂ atmosphere for 24 h. NIR-Silica NPs solutions with different concentrations from 0.5 to 1000 μ g/mL were added to each well, and the cells were subjected to an MTT assay after being incubated for another 24 h. The same concentration of the IR-780 micelle and IR-780 was set as the control.

Animal Tumor Models

BALB/c nude mice (4–6 weeks old weighing 20–25 g) were purchased from the Animal Center of Xi'an Jiaotong University and all animals received care in compliance with institutional guidelines. The procedures were approved by the Xian Jiaotong University Animal Care and Use Committee. To set up the tumor model, A431 cells (1×10^7) were inoculated into the mice by subcutaneous injection. When subcutaneous tumor masses developed to approximately 70–100 mm³, mice were divided into two groups randomly.

Fluorescence Intensity and Enhancement of Penetration Ability *In Vitro* and *In Vivo*

Fluorescence spectra were recorded on both free IR-780, IR-780 micelle and NIR-Silica NPs using a fluorescence spectrometer (DU730, Beckman, USA) with an excitation wavelength of 780 nm, and both excitation and emission slits were at 5 nm. The fluorescent images were obtained using a Xenogen IVIS Spectrum optical imaging device (PerkinElmer Inc.). The NIR-Silica NPs and IR-780 micelle solution (50 μ L) was added to 950 μ L DMSO as the experimental sample respectively. The DMSO solution with the same concentration of IR-780 was used as a control. For *in vitro* experiments, the NIR-Silica NPs, IR-780 micelle and free IR-780 dye samples were kept in a 2 mL tube. NIR fluorescent images of these samples were acquired using a 780 nm excitation light source and an 845 nm band-pass emission filter (0.2 s exposure time). To further confirm the fluorescence intensity in tissues, we carried out a subcutaneous injection experiment using mice (on the middle, left flanks and right flanks). Mice were injected with NIR-Silica NPs (middle), IR-780 micelle (left flanks) and free IR-780 dye (right flanks) formulation (both containing 50 μ L and 5 μ g/mL of the IR-780 dye).

The mice were imaged by the Xenogen IVIS system. Mice were anesthetized with pentobarbital and maintained in an anesthetized state during imaging procedures.

Sentinel Lymph Node Imaging *In Vivo*

NIR-Silica NPs, IR-780 micelle and IR-780 dye (both containing 50 μ L and 5 μ g/mL of the IR-780 dye) were injected intradermally into the forepaw foot pads of the three groups of mice respectively (experimental group with the injection of NIR-Silica NPs and the control group with the injection of the IR-780 micelle and IR-780). Mice were anesthetized with pentobarbital and maintained in an anesthetized state during imaging procedures. Five minutes and 30 minutes after the injection, the mice were imaged by the IVIS imaging system using a 780 nm excitation light source and an 845 nm band-pass emission filter (0.2 s exposure time). All images were processed with the IVIS imaging system.

Tumor Accumulation and Long-Term Imaging *In Vivo*

The long-term *in vivo* NIR fluorescent images of the NIR-Silica NPs were obtained using the Xenogen IVIS system. When the tumor volumes reached approximately 50 mm³, the mice were divided into three groups: free dye group, IR-780 micelle group and NIR-Silica NPs group. The samples (both containing 50 μ L and 5 μ g/mL of the IR-780 dye) were injected into the nude mice via tail vein. Images were taken at 1 h, 3 h, 5 h, 1 d, 2 d, 3 d, 5 d, 7 d and 10 d after injection using the *in vivo* imaging system mentioned above. The exposure time was set to 0.2 s. The nude mice were sacrificed 10 d after injection. The organs including lungs, heart, liver, spleen, kidneys and tumors were collected and analyzed by the IVIS imaging system.

Pathological Examination of Tissues

The excised tumors and organs were fixed in 4% paraformaldehyde solution for 1 day. These tissues were then embedded in paraffin and cut into 5 μ m thick sections. The sections were stained with hematoxylin-eosin (H&E) and examined using a digital microscope.

Statistical Analysis

The data are given as mean \pm SD deviation. Two groups were compared using a *t*-test. A *p*-value < 0.05 was considered as a statistically significant difference between the compared data.

RESULTS AND DISCUSSION

Synthesis and Characterization of NIR-Silica NPs

The NIR-Silica NPs were prepared using an improved method based on silica cross-linked micelles,²³ which is described briefly as follows and outlined in Figure 1. Initially, IR-780 and F-127 block copolymers were dissolved

completely in dichloromethane. After the solvent was evaporated to form a homogeneous mixture by means of gentle nitrogen flow under a vacuum at room temperature, the solid residue was then injected into a hydrochloric solution with magnetic stirring. With the polarity of the solution changes to acid abruptly, the F-127 block copolymers can immediately form a micellar core–shell structure.^{29,30} With the TEOS hydrolysis, the encapsulation of TEOS can be confined at the surface region between the core and the shell of the F-127 micelles.^{31,32} In order to control the silicate thickness and particle growth to strengthen the micellar structure, the addition of a small amount of DEDMS (5 wt% according to the total amount of F127 and TEOS) is important.^{33,34} Hence, by employing the silica cross-linked micelles, IR-780 molecules are encapsulated inside the core–shell structure, forming a transparent and clear aqueous suspension of IR-780 loaded silica cross-linked NPs (NIR-Silica NPs). Neither aggregation nor precipitation were observed over the entire period of experiments (more than six months). Such good stability can be mainly attributed to the PEO chains on the surface of the NIR-Silica NPs, which function as a steric stabilizer to keep the particles from agglomeration.³⁰ These results also indicate that the IR-780 dyes were successfully encapsulated inside the core of the NIR-Silica NPs. Moreover, the calculated encapsulation efficiency and drug loading are $83.5 \pm 2.37\%$ and $4.29 \pm 0.16\%$ after synthesis optimization according to mean particle size and polydispersityindex (PDI) of NIR-Silica NPs. Meanwhile, NIR-Silica NPs are characterized by FT-IR and thermal gravimetric analysis (TGA), and the results are shown in Figures 2 and 3. From Figure 2, the presence of absorption centered at 1080 cm^{-1} assigned to Si–O–Si species suggests the silica polymerized successfully. Moreover, NIR-Silica NPs exhibit a resistance to heat which is significantly greater than that of the IR-780 micelle, with a difference of about $\sim 100\text{ }^{\circ}\text{C}$ observed in Figure 3 at which maximum weight

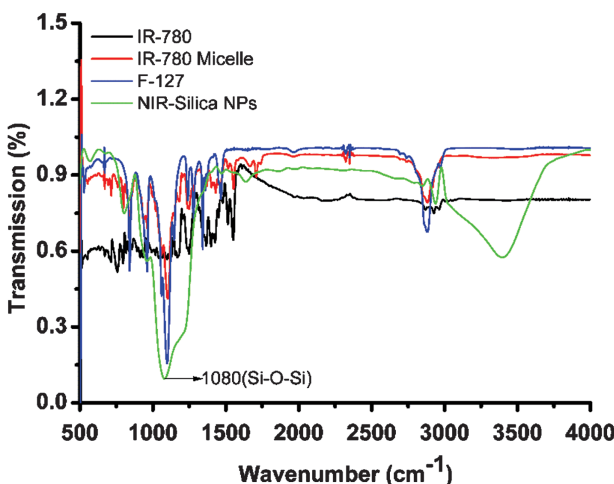


Figure 2. FT-IR spectra of the NIR-Silica NPs.

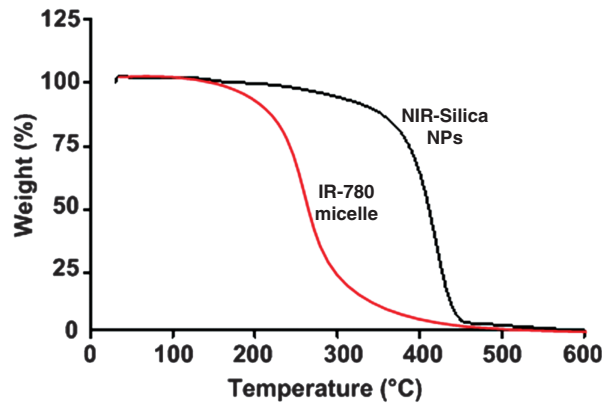


Figure 3. Thermal gravimetric analysis (TGA) of the NIR-Silica NPs and IR-780 micelle.

loss occurred. This improved stability can be rationalized by the presence of extensive silica cross-linking.

Transmission electron microscopy (TEM) images of the morphology of the NIR-Silica NPs are shown in Figure 4(A). The NPs possess a core–shell structure. The NIR-Silica NPs are discrete and uniform with a diameter of approximately 25 nm. In addition to TEM, the average

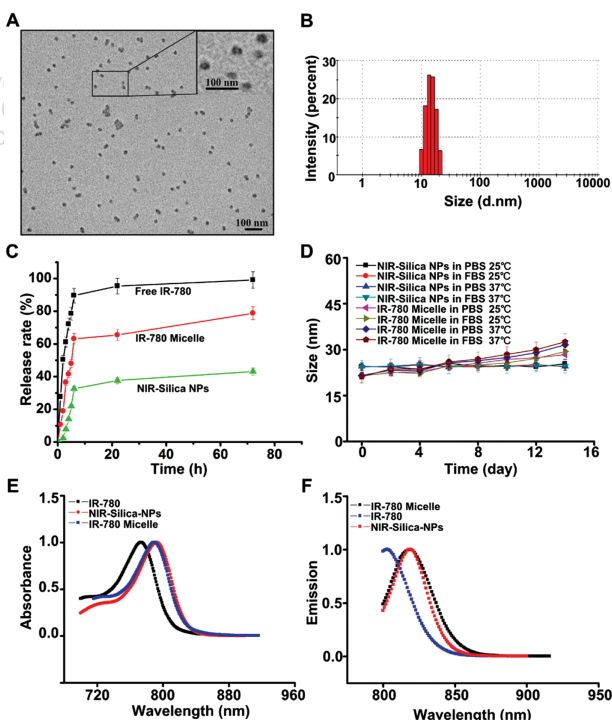


Figure 4. Characterization of NIR-Silica NPs. (A) TEM image of NIR-Silica NPs. (B) the size distribution of NIR-Silica NPs by DLS. (C) *In vitro* release profile of IR-780 micelles and NIR-Silica NPs after 72h ($n = 3$). (D) The size stability of NIR-Silica NPs and IR-780 micelle in PBS and 10% FBS varies with time and different temperatures over two weeks ($n = 3$). (E) Absorbance spectra of NIR-Silica NPs, IR-780 micelle and IR-780. (F) Emission spectra of NIR-Silica NPs, IR-780 micelle and IR-780

particle size distribution of the NIR-Silica NPs were investigated by using dynamic light scattering (DLS). From Figure 4(B), we can see that the results were consistent with the TEM observation above, since there was no significant difference in the hydrodynamic diameter of NIR-Silica NPs regardless of the encapsulated IR-780, which was in the range of 20–30 nm with relatively narrow size distribution. The results was similar to the reported hydrodynamic diameters of pure F-127 micelles (20–30 nm), indicating that the silica cross-linking did not change the size of the polymeric micelles.³⁵

Evaluation of IR-780 release was conducted by using dialysis method in which the NPs were dialyzed against a phosphate buffer solution ($\text{pH} = 7.4$) at 37°C . In all experiments, identical parameters were kept for the same group of experiments.^{34,36} Figure 4(C) shows the release profile of free IR-780, IR-780 micelles and NIR-Silica NPs. The results suggest that free IR-780 and IR-780 micelles have a much faster release profile than NIR-Silica NPs with 99% release of free IR-780, 78% release from IR-780 micelles and 43% release from NIR-Silica NPs in 72 hrs. Meanwhile, this result also implies that the NIR-Silica NPs are adequate to maintain and deliver the IR-780 for a long period. Meanwhile, the stability of NIR-Silica NPs was also investigated in PBS and 10% FBS at different temperatures and is shown in Figure 4(D). The results indicated that the particle size of the NIR-Silica NPs did not change significantly after two weeks in different media, and the solution remained clear without any precipitation. On the contrary, the size of the IR-780 micelle increased slightly, and the solution had a small amount of precipitation. Hence, the absorption spectrum was also recorded to confirm the result.

As far as we know, the optical properties of IR-780 are strongly dependent on the physical length and conformation of IR-780 chains. Figure 4(E) shows the absorption spectra of the NIR-Silica NPs and IR-780 micelle measured at the same IR-780 concentration in DMSO. It can be seen that the NIR-Silica NPs and IR-780 micelle have significantly broader absorption spectra than the free IR-780 dye in DMSO solution. The 15 nm broadening of absorption spectra is mainly attributed to the encapsulation of the IR-780 chains into the core of the NIR-Silica NPs because the absorption spectrum is mainly from the collective absorption of IR-780 chains with different conjugation lengths. Meanwhile, Figure 4(F) compares the fluorescent spectra behavior of the aqueous solution of NIR-Silica NPs and IR-780 micelle with that of the IR-780 solution in DMSO. It was observed that there was a significant 20 nm red-shift in the emission peak of the NIR-Silica NPs and IR-780 micelle compared with the IR-780 dye in DMSO. The red-shift of the NIR-Silica NPs can be attributed to the increased inter-chain interactions which occur because the encapsulation of the IR-780 chain into the core of the NIR-Silica NPs. These interactions allow for energy transfer from high energy to lower energy,

which lead to the red-shift of the NIR-Silica NPs. More importantly, this red shift induces two benefits for *in vivo* animal imaging. The first one is that the excitation and emission light of a longer wavelength (closer to the center of the optical window) are less attenuated by biological tissues.³⁷ The second benefit is the increased difference between the peak excitation and emission wavelengths, which is of great help in distinguishing the excitation signal from the emission one in the detection device.

The Fluorescence Intensity of NIR-Silica NPs *In Vitro and In Vivo*

The brightness of the fluorescent signal in the particles depends on the concentration of the encapsulated dye molecules, the quantum yield of the dye, its extinction coefficient, dye association and aggregation, and the scattering of excitation light by the particles.³⁸ Due to the silica specific nano-environment, the organic fluorescent dyes did not lose their fluorescence activity when a rather high concentration was reached inside the NPs by physically entrapment. Typically, dye molecules at those concentrations quench their fluorescence in the same volume of water. However, the quantum yield of the encapsulated dye still remains unchanged while the extinction coefficient of the particles increases several hundred times compared to the individual dye molecules. As a result, the particles can be up to two orders of magnitude brighter than polymeric particles of the same size assembled with organic dyes.²⁶ To verify the brightness of the synthesized particles, we measured the difference in fluorescence intensity between the free dye and NIR-Silica NPs. Figure 5(A) shows the fluorescent images of three EP tubes containing different concentrations of NIR-Silica NPs, IR-780 micelle and IR-780 dye respectively (left: NIR-Silica NPs; middle: IR-780 micelle; right: IR-780 dye). This showed that the fluorescence intensity of NIR-Silica NPs was clearly stronger than that of the IR-780 micelle and IR-780 dye at all of the observed concentrations, but the emission spectrum remains unchanged. To quantitatively describe this difference in intensity, a representative region of interest (ROI) was extracted from each fluorescent image and then the average intensity of each ROI was calculated. Figure 5(B) presents these average intensities as a function of the particle concentration, which quantitatively illustrates the intensity enhancement of NIR-Silica NPs over the IR-780 micelle and IR-780 dye, with the enhanced ratio being approximately 5–7 fold. For *in vivo* confirmation, the white light and fluorescent images of the mouse after subcutaneous dye, IR-780 micelle or NIR-Silica NPs injection were measured as shown in Figures 5(C and D). From Figure 5(D), clearly stronger signals were obtained at the side of the subcutaneous injection of NIR-Silica NPs. Thus, both *in vitro* and *in vivo* investigations showed that the fluorescence intensity could be greatly enhanced by using NIR-Silica NPs, which indicates the promise of NIR-Silica NPs as imaging agents because the higher the

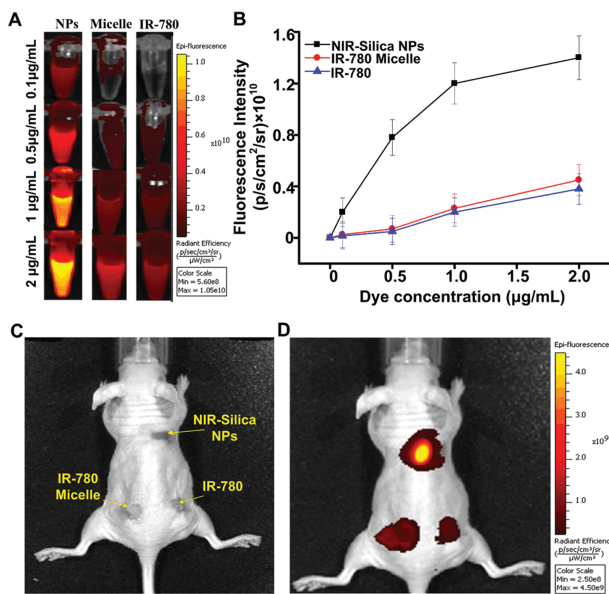


Figure 5. The fluorescence intensity of NIR-Silica NPs, IR-780 micelle and IR-780 dye *in vitro* and *in vivo*. (A) Color and fluorescent images of NIR-Silica NPs, IR-780 micelle and free IR-780 dye in vials. (B) The plots of fluorescence intensity of different concentrations of the complex between NIR-Silica NPs, IR-780 micelle and IR-780 ($n = 3$). (C) Photograph of a mouse after subcutaneous tumor injection. (D) NIR image of mice during 780 nm laser irradiation 5 min after subcutaneous injection with NIR-Silica NPs (middle), IR-780 micelle (left flanks) and IR-780 (right flanks).

fluorescence intensity, the better the penetration depth in biological tissues.

Cytotoxicity and Toxicity of NIR-Silica NPs *In Vitro and In Vivo*

It is well-known that the biocompatibility of fluorescent NPs is a critical issue for their use in clinical application. To study the biocompatibility of NIR-Silica NPs, the potential toxicity of NIR-Silica NPs was measured by incubating tumor cells (A431) and normal cells (HEK293) with NIR-Silica NPs at various concentrations for 24 and 48 h. No obvious cytotoxicity of NIR-Silica NPs from 0.5 to 1000 $\mu\text{g}/\text{mL}$ was observed. The results are shown in Figure 6, where Figures 6(A and C) present cytotoxicity results in A431 cells, while Figures 6(B and D) are those of HEK 293 cells; Figures 6(A and B) show the cell viability after 24 h incubation with IR-780, IR-780 micelle and NIR-Silica NPs respectively, and Figures 6(C and D) show those after 48 h incubation. We found that cell viability in each line after 24 h and 48 h incubation with the NPs was above 80% even at the highest tested concentrations of 1.0 mg/ml, demonstrating that the synthetic NPs had very low cytotoxicity supporting their safety. To further investigate the potential toxicity of NIR-Silica NPs, the NIR-Silica NPs (30 mg/Kg) was injected into healthy BALB/c mice via tail vein. PBS, the same dose of IR-780

and IR-780 micelle were set as the controls. Two weeks after injection, mice were then sacrificed and major organs (heart, liver, spleen, lungs, and kidneys) were sliced and stained by hematoxylin and eosin (H&E) for histology analysis. The results revealed that there was no noticeable tissue damage in all major organs of mice at the therapeutic dose (30 mg/Kg) in comparison with the control group. Meanwhile, some serum biochemistry assays were also conducted to assess the potential toxicity of NIR-Silica NPs. The main liver function markers including amino-transferase (ALT), aspartate aminotransferase (AST), alkaline phosphatase (ALP), adenosine deaminase (ADA) as well as kidney function markers including serum urea (UREA) and serum creatinine (CREA) were all measured. All of these results were obtained at 14d post-injection and did not show a significant difference with the control group. These results suggested no obvious hepatic or kidney disorder in the mice induced by NIR-Silica NPs intravenous injection.

In Vivo Imaging of Sentinel Lymph Nodes

SLN mapping in cancer plays an important role in the identification of micro-metastases in many patients and assessment of pathological staging and treatment.³⁹ IR-780 iodide, with a higher fluorescence emission and many unique optical properties compared with ICG in serum, has been successfully applied to SLN mapping.⁴⁰ As mentioned in the above results, the NIR-Silica NPs, with the enhanced fluorescent intensity ratio of about 5~7 over the IR-780 dye, should suitable for *in vivo* mapping of SLN. To confirm this concept, *in vivo* imaging of SLN was performed. In both the experimental and control groups, a similar ultralow dose of IR-780 (50 μL and 5 $\mu\text{g}/\text{mL}$) was injected into the paws of mice and lymph vessels from the injection site toward the SLN could be identified as early as 5 min after the injection of particles using the IVIS image system with 0.2 seconds exposure time. The fluorescence from the SLN could be clearly detected in the experimental group (Fig. 7(A)), but was not visualized clearly in the control group injected with only the IR-780 dye. The SLN contrast in both groups decreased gradually over time. Most importantly, the SLN could not be clearly visualized after 30 min in the control group, while fluorescence signals were still detectable in the experimental group. From Figure 7(B), we found that a much higher SLN fluorescence intensity was obtained in the experimental group than in the control, which was consistent with the fluorescence intensity enhancement investigation data. On the other hand, due to their small size and biocompatibility, NIR-Silica NPs could be completely cleared from the circulation and are not readily trapped by the reticular endothelium of the liver or spleen. Thus, the NIR-Silica NPs have a longer residence time in the body than IR-780 alone and can yield much higher signal-to-noise ratios with negligible background fluorescence due to serum protein binding, suggesting that the NIR-Silica NPs may be

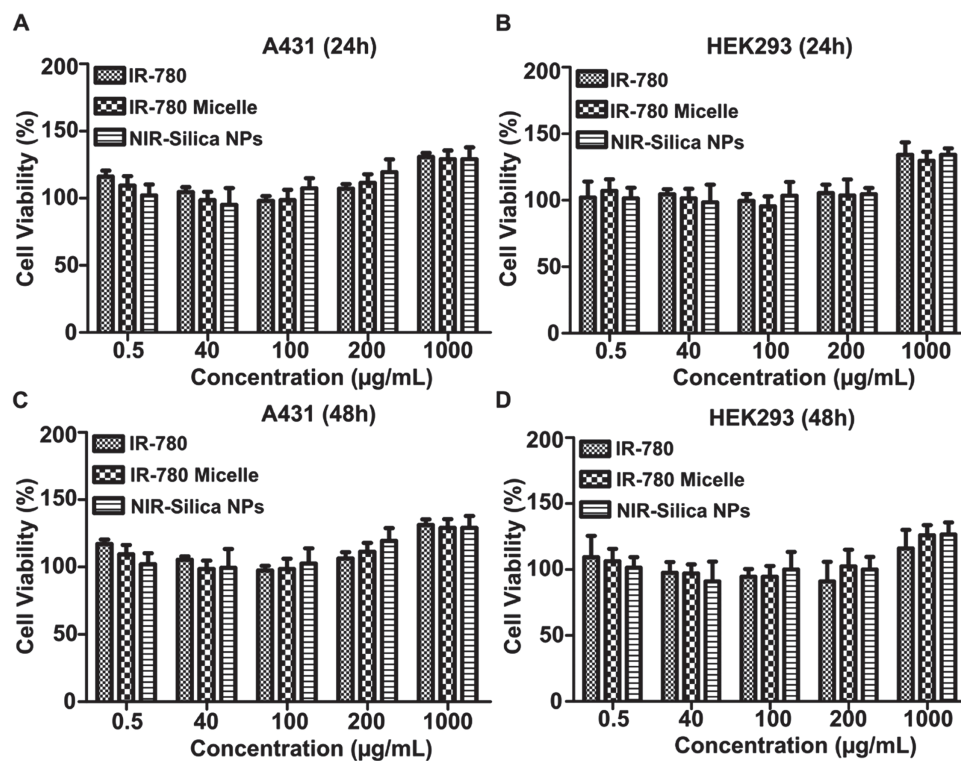


Figure 6. Cytotoxicity of NIR-Silica NPs *in vitro*. (A) Cell viability of A431 cells incubated with different concentrations of NIR-Silica NPs for 24 h. (B) Cell viability of HEK293 cells incubated with different concentrations of NIR-Silica NPs for 24 h. (C) Cell viability of A431 cells incubated with different concentrations of NIR-Silica NPs for 48 h. (D) Cell viability of HEK293 cells incubated with different concentrations of NIR-Silica NPs for 48 h. IR-780 and IR-780 micelle as the controls in all of the experiments.

a promising approach for *in vivo* imaging of SLN in the clinic.

Long Term Tumor Imaging *In Vivo*

For tumor imaging, it is important not only to develop safe and bright fluorescent probes but also to functionalize them to enhance their long-term potential in tumor imaging. To investigate whether NIR-Silica NPs could be used for long-term *in vivo* tumor imaging, they were injected intravenously into BALB/c mice bearing subcutaneous A439 tumors. The fluorescent images merged with white light

images of mice at various post-injection time-points over 10 days are presented in Figures 8(A–C) for both the NIR-Silica NPs, IR-780 micelle and IR-780 dye groups. It should be specifically mentioned that the fluorescence signals generated around the tumor at the post-injection time-point of 1 h in the NIR-Silica NPs and IR-780 micelle group could be easily observed, but no visible signals could be seen in the IR-780 dye group. At a post-injection time-point of 3 h, the fluorescence signals reached maximum intensity for both groups. The fluorescent intensity of the NIR-Silica NPs group was much higher than in the

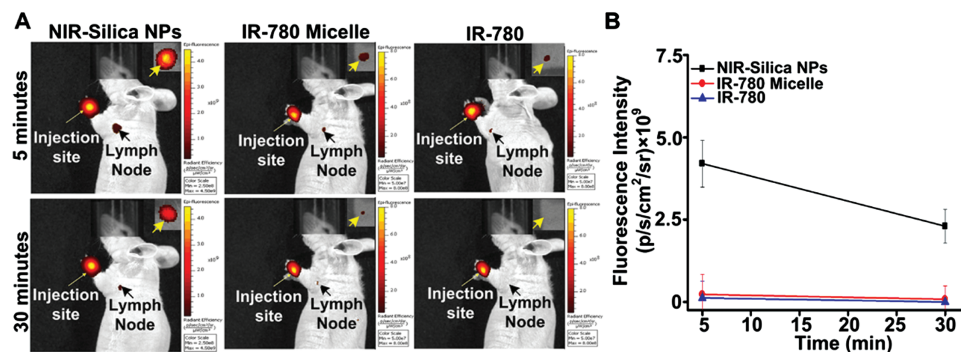


Figure 7. SLN imaging after intradermal injection of NIR-Silica NPs, IR-780 micelle and free IR-780. (A) Fluorescent images at 5 minutes and 30 minutes post-injection with NIR-Silica NPs, IR-780 micelle and IR-780. Inserted images after the injection sites were covered. (B) The plots of fluorescence intensity at different times between NIR-Silica NPs, IR-780 micelle and IR-780.

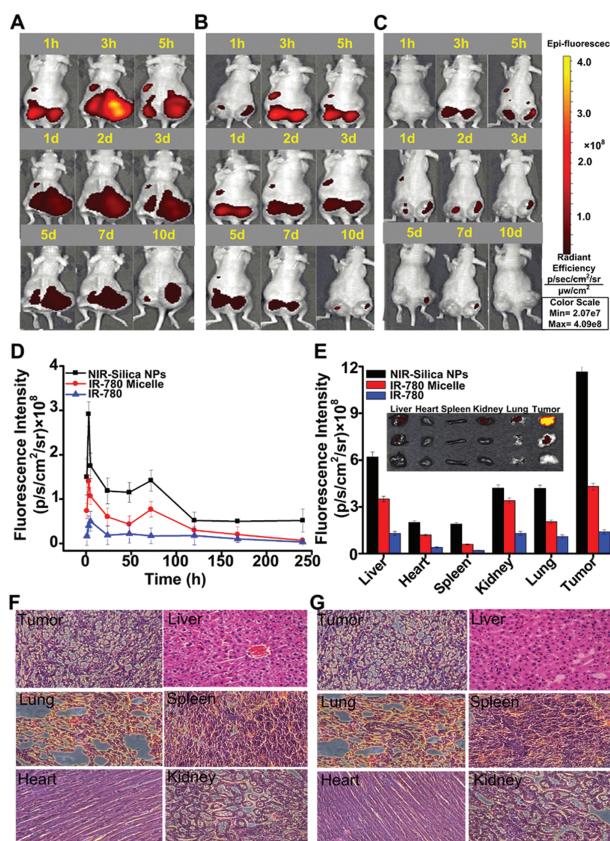


Figure 8. Long-term tumor imaging *in vivo*. (A) NIR-Silica NPs *in vivo* images taken over a 10 day period. (B) IR-780 micelle *in vivo* images taken over a 10 day period. (C) Free IR-780 dye *in vivo* images taken over a 10 day period. (D) The plot of the relationship between the normalized intensity around the tumor and injection time point. (E) The fluorescent images of organs and tumors in A431 tumor-bearing mice after 10 days post-injection of NIR-Silica NPs, IR-780 micelle and IR-780. (F) H&E stained images of major organs including tumors, liver, heart, spleen, lungs and kidneys. Healthy mice were treated with saline as controls. (G) H&E stained images of major organs including tumors, liver, heart, spleen, lungs and kidneys. Healthy mice treated by NIR-Silica NPs (50 μ l and 5 μ g/ml) as the experimental group.

IR-780 micelle and IR-780 dye group. At a post-injection time-point of 10 days, there were no detectable signals in the IR-780 dye group, while the fluorescence signals could also be visualized in the NIR-Silica NPs group. To quantitatively and intuitively display the intensity variation, a representative ROI was extracted for each fluorescent image by tumor area, and the average intensity inside each ROI was calculated. The average intensity as a function of the post-injection time of the particles is shown in Figure 8(D), where the black square line describes the intensity variation of NIR-silica NPs, the red circle line indicates the IR-780 micelle and the blue triangle line represents the IR-780 dye. After 10 days of longitudinal imaging, the three mice groups were all sacrificed and the main organs as well as the tumors were removed to

acquire fluorescent images, as shown in Figure 8(E). We found that very strong signals were observed in the tumors, whereas very weak or even no fluorescence signals could be detected in the main organs for the NIR-Silica NPs group, which could also be seen from the intensity distribution map shown in Figure 8(E). To further confirm this, major organs (tumor, liver, spleen, lungs, and kidneys) of the mice were sectioned and stained by H&E for histological analysis. The results revealed that there was no noticeable tissue damage in major organs of mice at a low dose of NIR-Silica-NPs (Figs. 8(F and G)). From Figure 8, some interesting observations can be made. First, the fluorescent signals detected in the NIR-Silica NPs group were much stronger than those in the IR-780 dye group, which is in accordance with the results obtained in other experiments. Furthermore, the NIR-Silica NPs showed strong signals in the tumor compared with the surrounding tissues, which provides evidence that the NIR-Silica NPs are potentially an excellent agent for tumor targeting and imaging. Second, the residence time of the NIR-Silica NPs in the body was much longer than that of the IR-780 dye; which this might be caused by the following two reasons. On the one hand, the NIR-Silica NPs gather around the tumor because of their smaller size, which allows the avoidance of clearance by the RES and enhances the EPR.⁴¹ On the other hand, it is well-known that small molecular weight dyes, such as IR-780, are rapidly cleared from the body.¹⁶ In contrast, NIR-silica NPs can protect the dye from degradation and then greatly extend its circulation time in the body.⁴² In summary, the NIR-Silica NPs showed stronger signals with good contrast between the tumor and surrounding tissues and demonstrated a longer circulation time in the imaging experiments, which further improved the weak signal and rapid degradation of IR-780 dye in physiological conditions. Preliminary results provided strong evidence that the NIR-Silica NPs are sufficient for longitudinal tumor imaging in the living body.

CONCLUSION

In this study, we described the development of a novel and simple method to generate a new family of biocompatible silica cross-linked micellar core–shell encapsulating IR-780 nanoparticles (NIR-Silica NPs), which were prepared by modifying a bio-inspired silification approach. The process is simple and robust such that it can simultaneously encapsulate IR-780 inside the core of the pluronic F-127 polymeric micelles and form a thin silica layer at the interfacial region between the core and the shell cross-linking the polymeric micelles. The NIR-Silica NPs possess distinct characteristics with an exceptionally small diameter and high fluorescence brightness. In addition, the NIR-Silica NPs also exhibit a high colloidal stability and very low cytotoxicity. Moreover, in a series of *in vivo* experiments including SLN mapping and long-term tumor imaging, results demonstrated the strong capability of

longer circulation time and metabolic stability for *in vivo* optical imaging. Meanwhile, the (PEO)-OH terminals on the surface of the NIR-Silica NPs' surface could improve their conjugation with biological molecules. More importantly, short exposure times could achieve a much higher signal-to-noise ratio at very low dye concentrations, suggesting the great potential of NIR-Silica NPs as a new fluorescence imaging agent for clinical application.

Conflict of Interest

The authors confirm that there are no known conflicts of interest associated with this publication. Funding sources had no involvement in study design; collection, analysis, and interpretation of data; writing of the report; and in the decision to submit the article for publication.

Acknowledgments: The authors acknowledge the financial support by the Program of National Basic Research and Development Program of China (973) under Grant No. 2011CB707702, the National Natural Science Foundation of China under Grant Nos. 81101100, 81227901, 81571725, 81230033, 81090272, 81101083, 31371006, 61405149, 81401442, the Natural Science Basic Research Plan in Shaanxi Province of China under Grant No. 2015JQ6249, and the Fundamental Research Funds for the Central Universities (NSIZ021402, NSIY061406).

Delivered by Ingenta to: University of Alberta
IP: 5.62.155.108 On: Wed, 01 Dec 2016
Copyright: American Society of Clinical Oncology

REFERENCES

- K. Yan, H. Li, P. Li, H. Zhu, J. Shen, C. Yi, S. Wu, K. W. Yeung, Z. Xu, and H. Xu, Self-assembled magnetic fluorescent polymeric micelles for magnetic resonance and optical imaging. *Biomaterials* 35, 344 (2014).
- Q. T. Nguyen and R. Y. Tsien, Fluorescence-guided surgery with live molecular navigation: A new cutting edge. *Nat. Rev. Cancer* 13, 653 (2013).
- A. Louie, Multimodality imaging probes: Design and challenges. *Chem. Rev.* 110, 3146 (2010).
- A. Yuan, J. Wu, X. Tang, L. Zhao, F. Xu, and Y. Hu, Application of near-infrared dyes for tumor imaging, photothermal, and photodynamic therapies. *J. Pharm. Sci.* 102, 6 (2013).
- L. Qi and X. Gao, Emerging application of quantum dots for drug delivery and therapy. *Expert Opin. Drug Deliv.* 5, 263 (2008).
- X. Zheng, D. Xing, F. Zhou, B. Wu, and W. R. Chen, Indocyanine Green-containing nanostructure as near infrared dual-functional targeting probes for optical imaging and photothermal therapy. *Mol. Pharm.* 8, 447 (2011).
- C. Zheng, M. Zheng, P. Gong, D. Jia, P. Zhang, B. Shi, Z. Sheng, Y. Ma, and L. Cai, Indocyanine green-loaded biodegradable tumor targeting nanoprobes for *in vitro* and *in vivo* imaging. *Biomaterials* 33, 5603 (2012).
- D. K. Kadavakkara, M. J. Korrer, J. W. Bulte, and H. I. Levitsky, Paradoxical decrease in the capture and lymph node delivery of cancer vaccine antigen induced by a TLR4 agonist as visualized by dual-mode imaging. *Cancer Res.* 75, 51 (2015).
- C. Zhang, S. Wang, J. Xiao, X. Tan, Y. Zhu, Y. Su, T. Cheng, and C. Shi, Sentinel lymph node mapping by a near-infrared fluorescent heptamethine dye. *Biomaterials* 31, 1911 (2010).
- J. Yu, D. Javier, M. A. Yaseen, N. Nitin, R. Richards-Kortum, B. Anvari, and M. S. Wong, Self-assembly synthesis, tumor cell targeting, and photothermal capabilities of antibody-coated indocyanine green nanocapsules. *J. Am. Chem. Soc.* 132, 1929 (2010).
- L. Yuan, W. Lin, K. Zheng, L. He, and W. Huang, Far-red to near infrared analyte-responsive fluorescent probes based on organic fluorophore platforms for fluorescence imaging. *Chem. Soc. Rev.* 42, 622 (2013).
- C. Zhang, T. Liu, Y. Su, S. Luo, Y. Zhu, X. Tan, S. Fan, L. Zhang, Y. Zhou, and T. Cheng, A near-infrared fluorescent heptamethine indocyanine dye with preferential tumor accumulation for *in vivo* imaging. *Biomaterials* 31, 6612 (2010).
- S. Luo, E. Zhang, Y. Su, T. Cheng, and C. Shi, A review of NIR dyes in cancer targeting and imaging. *Biomaterials* 32, 7127 (2011).
- E. Zhang, S. Luo, X. Tan, and C. Shi, Mechanistic study of IR-780 dye as a potential tumor targeting and drug delivery agent. *Biomaterials* 35, 771 (2014).
- C.-L. Peng, Y.-H. Shih, P.-C. Lee, T. M.-H. Hsieh, T.-Y. Luo, and M.-J. Shieh, Multimodal image-guided photothermal therapy mediated by 188Re-labeled micelles containing a cyanine-type photosensitizer. *ACS Nano* 5, 5594 (2011).
- C. Yue, P. Liu, M. Zheng, P. Zhao, Y. Wang, Y. Ma, and L. Cai, IR-780 dye loaded tumor targeting theranostic nanoparticles for NIR imaging and photothermal therapy. *Biomaterials* 34, 6853 (2013).
- A. Yuan, X. Qiu, X. Tang, W. Liu, J. Wu, and Y. Hu, Self-assembled PEG-IR-780-C13 micelle as a targeting, safe and highly-effective photothermal agent for *in vivo* imaging and cancer therapy. *Biomaterials* 51, 184 (2015).
- C. Jiang, H. Cheng, A. Yuan, X. Tang, J. Wu, and Y. Hu, Hydrophobic IR780 encapsulated in biodegradable human serum albumin nanoparticles for photothermal and photodynamic therapy. *Acta Biomater.* 14, 61 (2015).
- A. K. Singh, M. A. Hahn, L. G. Gutwein, M. C. Rule, J. A. Knapik, B. M. Moudgil, S. R. Grobmyer, and S. C. Brown, Multi-dye theranostic nanoparticle platform for bioimaging and cancer therapy. *Int. J. Nanomedicine* 7, 2739 (2012).
- A. Rösler, G. W. Vandermeulen, and H.-A. Klok, Advanced drug delivery devices via self-assembly of amphiphilic block copolymers. *Adv. Drug Delivery Rev.* 64, 270 (2012).
- E. S. Read and S. P. Armes, Recent advances in shell cross-linked micelles. *Chem. Commun.* 29, 3021 (2007).
- V. Biju, Chemical modifications and bioconjugate reactions of nanoparticles for sensing, imaging, drug delivery and therapy. *Chem. Soc. Rev.* 43, 744 (2014).
- J. Yuan, O. O. Mykhaylyk, A. J. Ryan, and S. P. Armes, Cross-linking of cationic block copolymer micelles by silica deposition. *J. Am. Chem. Soc.* 129, 1717 (2007).
- V. Mamaeva, C. Sahlgren, and M. Linden, Mesoporous silica nanoparticles in medicine-recent advances. *Adv. Drug Delivery Rev.* 65, 689 (2013).
- I. Sokolov, and S. Naik, Novel fluorescent silica nanoparticles: Towards ultrabright silica nanoparticles. *Small* 4, 934 (2008).
- E. B. Cho, D. O. Volkov, and I. Sokolov, Ultrabright fluorescent mesoporous silica nanoparticles. *Small* 6, 2314 (2010).
- S. Palantavida, R. Tang, G. Sudlow, W. Akers, S. Achilefu, and I. Sokolov, Ultrabright NIR fluorescent mesoporous silica nanoparticles. *Journal of Materials Chemistry B* 2, 3107 (2014).
- E. B. Cho, D. O. Volkov, and I. Sokolov, Ultrabright fluorescent silica mesoporous silica nanoparticles: Control of particle size and dye loading. *Adv. Funct. Mater.* 21, 3129 (2011).
- Q. Hu, E. V. van Gaal, P. Brundel, H. Ippel, T. Hackeng, C. J. Rijcken, G. Storm, W. E. Hennink, and J. Prakash, A novel approach for the intravenous delivery of leuprolide using core-cross-Linked polymeric micelles. *J. Controlled Release* 205, 98 (2015).
- R. Basak, and R. Bandyopadhyay, Encapsulation of hydrophobic drugs in pluronic F127 micelles: Effects of drug hydrophobicity, solution temperature, and pH. *Langmuir* 29, 4350 (2013).

31. H. Tan, Y. Zhang, M. Wang, Z. X. Zhang, X. H. Zhang, A. M. Yong, S. Y. Wong, A. Y.-C. Chang, Z. K. Chen, X. Li, M. Choolani, and J. Wang, Silica-shell cross-linked micelles encapsulating fluorescent conjugated polymers for targeted cellular imaging. *Biomaterials* 33, 237 (2012).
32. J. E. Lofgreen and G. A. Ozin, Controlling morphology and porosity to improve performance of molecularly imprinted sol-gel silica. *Chem. Soc. Rev.* 43, 911 (2014).
33. S. Kumar, J.-F. Allard, D. Morris, Y. L. Dory, M. Lepage, and Y. Zhao, Near-infrared light sensitive polypeptide block copolymer micelles for drug delivery. *J. Mater. Chem.* 22, 7252 (2012).
34. Q. S. Huo, J. Liu, L. Q. Wang, Y. B. Jiang, T. N. Lambert, and E. Fang, A new class of silica cross-linked micellar core–shell nanoparticles. *J. Am. Chem. Soc.* 128, 6447 (2006).
35. W. Cao, Y. Gu, M. Meineck, T. Li, and H. Xu, Tellurium-containing polymer micelles: Competitive-ligand-regulated coordination responsive systems. *J. Am. Chem. Soc.* 136, 5132 (2014).
36. X. Hao, M. Zhou, X. Zhang, J. Yu, J. Jie, C. Yu, and X. Zhang, Highly luminescent and photostable core–shell dye nanoparticles for High Efficiency Bioimaging. *Chem. Commun. (Camb.)* 50, 737 (2014).
37. Y. Ma, S. Tong, G. Bao, C. Gao, and Z. Dai, Indocyanine green loaded SPIO nanoparticles with phospholipid-PEG coating for dual-modal imaging and photothermal therapy. *Biomaterials* 34, 7706 (2013).
38. Y.-W. Noh, H. S. Park, M.-H. Sung, and Y. T. Lim, Enhancement of the photostability and retention time of indocyanine green in sentinel lymph node mapping by anionic polyelectrolytes. *Biomaterials* 32, 6551 (2011).
39. Y.-W. Noh, S.-H. Kong, D.-Y. Choi, H. S. Park, H.-K. Yang, H.-J. Lee, H. C. Kim, K. W. Kang, M.-H. Sung, and Y. T. Lim, Near-infrared emitting polymer nanogels for efficient sentinel lymph node mapping. *ACS Nano* 6, 7820 (2012).
40. S. Jiang, M. K. Gnanasammudhan, and Y. Zhang, Optical imaging-guided cancer therapy with fluorescent nanoparticles. *J. Royal Soc. Interface.* 7, 3 (2010).
41. R. K. Kainthan, S. R. Hester, E. Levin, D. V. Devine, and D. E. Brooks, *In vitro* biological evaluation of high molecular weight hyperbranched polyglycerols. *Biomaterials* 28, 4581 (2007).
42. S. Palantavida, N. V. Guz, C. Woodworth, and I. Sokolov, Ultrabright Fluorescent mesoporous silica nanoparticles for prescreening of cervical cancer, Nanomedicine: Nanotechnology. *Biology and Medicine.* 9, 1255 (2013).

Delivered by Ingenta to: University of South Carolina
IP: 5.62.155.108 On: Wed, 01 Mar 2017 03:25:17
Copyright: American Scientific Publishers